Novel mechanistic view of catalytic ozonation of gaseous toluene by dual-site kinetic modeling

Maocong Hu, Zhenhua Yao, K.N. Hui, K.S. Hui

PII: S1385-8947(16)31330-4
DOI: http://dx.doi.org/10.1016/j.cej.2016.09.086
Reference: CEJ 15796

To appear in: *Chemical Engineering Journal*

Received Date: 25 May 2016
Revised Date: 15 September 2016
Accepted Date: 16 September 2016

Please cite this article as: M. Hu, Z. Yao, K.N. Hui, K.S. Hui, Novel mechanistic view of catalytic ozonation of gaseous toluene by dual-site kinetic modeling, *Chemical Engineering Journal* (2016), doi: http://dx.doi.org/10.1016/j.cej.2016.09.086

Novel mechanistic view of catalytic ozonation of gaseous toluene by dual-site kinetic modeling

Maocong Hu[a], Zhenhua Yao[a], K.N. Hui[b,*], K.S. Hui[c,**]

[a] Department of Chemical, Biological and Pharmaceutical Engineering, New Jersey Institute of Technology, Newark, NJ 07102, USA

[b] Institute of Applied Physics and Materials Engineering, University of Macau, Avenida da Universidade, Taipa, Macau

[c] School of Mathematics, University of East Anglia, Norwich, NR4 7TJ, United Kingdom

[*] Corresponding author

Email addresses: bizhui@umac.mo (K.N. Hui)

Tel: +853-8822-4426; Fax: +853-8822-2426

[**]Corresponding author

E-mail: k.hui@uea.ac.uk (K.S. Hui)

Tel: +44 (0) 1603 592600

Abstract

The catalytic ozonation of VOCs is a promising approach for degradation of indoor VOCs, such as gaseous toluene. However, the mechanism and relevant kinetic steps involved in this reaction remain unclear. In this study, the catalytic ozonation of toluene over MnO_2/graphene was investigated using the empirical power law model and classic Langmuir-Hinshelwood single-site (denoted as L-H_s) mechanism. The apparent activation energy determined using the power law model was 29.3±2.5 kJ mol^{-1}. This finding indicated that the catalytic ozonation of toluene over MnO_2/graphene was a heterogeneous reaction, and the Langmuir-Hinshelwood mechanism was applicable. However, the L-H_s mechanism did not fit the experimental data, suggesting that the reaction was non-single-site governed. A novel Langmuir-Hinshelwood dual-site (denoted as L-H_d) mechanism was then proposed to explain the experimental observations of the catalytic ozonation of toluene over MnO_2/graphene through a steady-state kinetic study. This mechanism was based on the hypothesis that MnO_2 was responsible for ozone decomposition and toluene adsorption on graphene; these two types of adsorption were coupled by an adjacent attack. Furthermore, XPS results confirmed the presence of a strong connection between MnO_2 and graphene sites on the surface of MnO_2/graphene. This connection allowed the adjacent attack and validated the dual-site mechanism. The L-H_d model was consistent with the predicted reaction rate of toluene removal with a correlation coefficient near unity (r^2 = 0.9165). Moreover, the physical criterion was in accordance with both enthalpy and entropy of toluene adsorption constraints. Fulfillment of mathematical and physical criteria indicated the catalytic ozonation of toluene over MnO_2/graphene can be well described by the L-H_d mechanism. This study helps understand the catalytic ozonation of toluene over MnO_2/graphene in a closely mechanistic view.

Keywords: MnO_2/graphene, toluene degradation, catalytic ozonation, Langmuir-Hinshelwood dual-site mechanism, kinetic modelling

Nomenclature

X_{tol}	conversion of toluene	$C_{tol,0}$	concentrations of toluene at the feed
C_{tol}	concentrations of toluene at outlet	r_{tol}	steady-state reaction rates of toluene,
C_{O_3}	steady-state concentrations of ozone	W	catalyst weight
v	total gas flow rate	E_a	activation energy
A	pre-exponential factor	ΔS_{tol}	toluene adsorption entropy
ΔS^0_g	standard gas phase entropy	ΔH_{tol}	toluene adsorption enthalpy
R	universal gas constant	T	temperature in Kelvin (K)
k_i	reaction rate constant	K_{tol}	adsorption equilibrium constant
r_{cal}	predicted reaction rates	r_{exp}	experimental reaction rates
r^2	correlation coefficient	$s1$	MnO_2 active sites
$s2$	graphene active sites		

1. Introduction

Toluene, a volatile organic compound (VOC), is carcinogenic and harmful to human health [1-4]. Catalytic ozonation is a promising approach used to degrade VOCs [5-9]. The catalytic ozonation of VOCs is considered a surface reaction, which follows the Langmuir-Hinshelwood mechanism and comprises adsorbed VOC molecules and atomic oxygen species; this process was originally proposed by Oyama et al. [10] to investigate the kinetics and mechanism of the catalytic ozonation of acetone over MnO_x/SiO_2 by combining in situ Raman spectroscopy with transient kinetics techniques. To the best of our knowledge, Oyama et al. study is the only systematic study on the kinetics and mechanism of the catalytic ozonation of VOCs, which has been widely used to explain the experimental results of the catalytic ozonation of several VOCs, such as toluene [11, 12], propanol [13], benzene [14], and cyclohexane [15]. Moreover, the Langmuir-Hinshelwood dual-site (L-H_d) mechanism was proposed to explain the elementary steps involved in the reaction [10], in which the SiO_2 support was applied for acetone adsorption, whereas ozone was adsorbed on MnO_x. However, only one site (MnO_x) was involved in the derivation of the proposed kinetic model; thus, the derived kinetic equation was actually based on the Langmuir-Hinshelwood single-site (denoted as L-H_s) mechanism.

Although numerous studies were conducted on the catalytic ozonation of VOCs [16-23], the underlying mechanism and its relevant kinetic steps remain unclear [24]. Other than the recent study by Rezaei and Soltan [24], no studies were performed to test the validity of the L-H_s mechanism on the catalytic ozonation of toluene over alumina-supported manganese oxide catalysts. The toluene activation step in this model differs from that proposed by Oyama et al. [10]. Moreover, the model was established based on the assumption that toluene is activated by extracting hydrogen from the methyl group of toluene, and C–H bond cleavage is

the relevant kinetic step for catalytic ozonation of toluene. The derived rate expression from this assumption is identical to that based on the power law reported in the same study [24]. The researchers also suggested that additional techniques, including in situ spectroscopy, isotopic exchange techniques, and density functional theory (DFT) calculations, must be performed to validate the proposed mechanism [24]. Nevertheless, positive adsorption entropy (100 J mol^{-1} K^{-1}) and enthalpy (8 kJ mol^{-1}) values were obtained, thereby indicating the occurrence of endothermic adsorption, which is uncommon for catalytic reactions [24, 25]. Two models [10, 24] were developed based on the L-H_s mechanism, in which surface reactions occurred only on active metal oxide sites. Supports, such as SiO_2 and alumina, served as platforms for active site dispersion, which were meaningless from the kinetic point of view of rate expression development.

In our previous study, we reported the reaction performance of MnO_2/graphene catalysts with different MnO_2 loading for catalytic ozonation of toluene [26]. On the basis of the reaction performance data and from the chemical point of view, the function of graphene was proposed not only as support for MnO_2 dispersion, where ozone adsorption occurred, but also as a toluene adsorption site because of the π-electron coupling between toluene and graphene. From the kinetic point of view, this dual role played by graphene, especially the latter, could be attributed to the non-competitive dual-site mechanism. In this mechanism, the MnO_2 sites are reserved for ozone adsorption according to a classical ozone decomposition mechanism [27, 28], whereas graphene offers sites for toluene adsorption. The L-H_d mechanism has been commonly used to understand catalytic reactions [29-32]; however, to the best of our knowledge, no studies were reported on understanding catalytic ozonation of VOCs by the L-H_d mechanism.

In this paper, we reported a kinetic study for catalytic ozonation of toluene over MnO_2/graphene. X-ray photoelectron spectroscopy (XPS) analysis was conducted to investigate the catalyst surface structure, and the results confirmed our previous study based on bulk phase characterization [26]. Well-designed kinetic reaction tests were also performed to collect reaction rate data under the steady state at three temperature points. Three kinetic rate models were then developed based on power law, Langmuir-Hinshelwood single-site mechanism, and Langmuir-Hinshelwood dual-site mechanism. These models were validated by statistically fitting the kinetic data obtained and were differentiated using both mathematical and physical criteria. Kinetic parameters, including apparent activation energy, activation energy, reaction rate constant, pre-exponential factor, adsorption equilibrium constant, and adsorption entropy and enthalpy, were determined and discussed. Based on the kinetic modelling results, one promising L-H_d mechanism was proposed for catalytic ozonation of toluene over MnO_2/graphene.

2. Experimental and data analysis

2.1. MnO_2/graphene preparation and characterization

The details of sample preparation were reported in previous study [26]. Briefly, 64.6 wt% MnO_2/graphene composite was synthesized using a redox reaction between the carbons of graphene oxide and potassium permanganate and the reduction of graphene oxide sheets to graphene sheets under hydrothermal conditions. This reaction can progress completely because MnO_4^- ions can interact with graphene oxide layers given the good hydrophilicity of graphene oxide [33].

Several characterization techniques are used to examine the bulk structure of the MnO_2/graphene catalyst in our previous work [26]. In this study, we investigated the surface

structure of MnO_2/graphene by XPS analysis and confirmed the connection between surface MnO_2 and graphene support, which renders the dual-site mechanism as feasible. XPS analysis was performed on ESCALab 220i-XL (VG Scientific) equipped with Ar^+ sputtering (5 keV) for depth profile analysis. Monochromatic Al Kα was used as radiation source, with the energy scale calibrated and corrected for charging using the C 1s (284.9 eV) line as the reference binding energy.

2.2. Steady-state kinetic study

All conversion data were collected with values less than 15% under all reaction conditions to obtain reliable data for reaction kinetics. The schematic of the setup was reported in our previous studies [26, 34, 35]. Briefly, the inlet section consisted of a specific concentration of toluene gas produced from a VOC generator (VICI Metronics Dynacalibrator, model 150, USA), with N_2 as carrier gas, as well as a specific concentration of ozone (volume flow rate of 50–250 mL/min) produced from O_2 (99.99%) through a silent discharge ozone generator (MEDOZONS Ltd., Medozons-BM-02, Russia) and a mixer. The inlet gas mixture was fed into a tube fixed-bed micro-reactor with a temperature controller (Harrick, model: HVC-DRP-3, USA) loaded with approximately 80 mg (volume of 0.11 cm^3) of the samples. To eliminate the mass-transfer effect, we selected a sample size of 100–150 mesh by providing the catalyst bed height to a catalyst particle size ratio of $L/D_p \geq 50$ and reactor internal diameter to a catalyst particle size ratio of $D/D_p \geq 30$ [36]. Catalytic ozonation of gaseous toluene over the MnO_2/graphene sample was performed at varied temperatures (295, 313, and 333 K) under atmospheric pressure. The total flow rate was set at 150 mL/min (i.e., 2.5×10^{-6} m^3 s^{-1}) for all runs with different toluene concentrations (300–800 ppm, i.e., 0.0124–0.0329 mol m^{-3}) and fixed ozone concentration (1600 ppm, i.e., 0.0659 mol m^{-3})

(Table 1).

Reactants in the inlet stream and products in the effluent stream were analyzed online by using a Fourier transform infrared (FTIR) spectrometer (Bruker, Model Tenser 27) equipped with a 10 cm path-length gas cell (Infrared Analysis, model: SP-10 cm, optical length = 10 cm, volume = 100 mL). The recorded spectra were the average of 16 scans at a resolution of 0.5 cm^{-1}. The conversion of toluene (X_{tol}) was calculated using Eq. (1), where $C_{tol,0}$ and C_{tol} represent the concentrations of toluene at the feed and outlet of the reactor, respectively, and the subscript "0" represents the feed condition. All data were collected under the steady-state condition (i.e., when the concentration of the outlet gas is kept constant). The average value of three sets of independent experiments (deviations within ±5%) was reported using three different batches of the sample. The steady-state reaction rate was calculated using Eq. (2), where r_{tol}, $C_{tol,0}$, v, X_{tol}, and W are the steady-state reaction rates of toluene, toluene feed concentration, total gas flow rate, steady-state toluene conversion, and catalyst weight, respectively.

$X_{tol} = \frac{C_{tol,0} - C_{tol}}{C_{tol,0}} \times 100\%$	(1)
$r_{tol} = \frac{C_{tol,0} v X_{tol}}{W}$	(2)

2.3. Data analysis

Three kinetic models were developed based on different mechanisms (*3.2 Kinetic Study* for details). Kinetic parameters (reaction rate constant k_i and adsorption equilibrium constant K_{tol}) were obtained by fitting each model to the experimental results by combining MATLAB R2014a by using curve-fitting applications with the Levenberg–Marquardt method and the Excel optimizer solver for estimated initial values [37-39]. For each model, after the kinetic

parameters were calculated for each temperature, Arrhenius and Van't Hoff equations were employed to determine the pre-exponential factor A, activation energy E_a, toluene adsorption enthalpy ΔH_{tol}, and adsorption entropy ΔS_{tol}, if applicable by using linear regression with Eqs. (3) and (4). R is the universal gas constant 8.314 $J\,K^{-1}\,mol^{-1}$, and T is the reaction temperature in Kelvin (K).

$\ln k_i = \ln A + \left(\frac{-E_a}{R}\right)\frac{1}{T}$	(3)
$\ln K_{tol} = \left(\frac{-\Delta H_{tol}}{R}\right)\frac{1}{T} + \frac{\Delta S_{tol}}{R}$	(4)

Criteria must be met for the models to mathematically converge with the experimental results and render the derived kinetic parameters as physically meaningful. First, the sum of squared errors between the measured data and the values derived from the kinetic models should be minimized as much as possible. As such, nonlinear least squares regression was used to calculate the reaction rates that would yield the minimum total squared error between the predicted and experimental data, as determined from Eq. 5 at each temperature point. The correlation coefficient (r^2) was then used to intuitively distinguish the derived model [40, 41].

$\min \sum_{1}^{n} (r_{exp.,n} - r_{cal.,n})^2$	(5)

where $r_{exp.}$ and $r_{cal.}$ represent the experimental and predicted reaction rates based on the kinetic model. The index n refers to the nth reaction rate at a specific temperature point and corresponds to specific toluene and ozone concentrations.

Second, satisfying the mathematical constraint was the first step for model discrimination. The physical meaning of the derived parameters was considered to select the optimal reaction model. Adsorption entropy and enthalpy should meet the following list of

criteria in Eqs. (6) and (7) for catalytic reactions [42-45].

$41.9 < -\Delta S^0_{ads} < \Delta S^0_g$	(6)
$-\Delta S^0_{ads} \leq 51.1 - 1.4\Delta H^0_{ads}$	(7)

Eq. (6) indicates that the loss of entropy $-\Delta S^0_{ads}$ in the adsorption onto the catalyst should be higher than 41.9 J mol^{-1} K^{-1} but lower than the standard gas phase entropy (320.7 J mol^{-1} K^{-1} for toluene) [46]. From Eq. (7), when a molecule is strongly bound to the catalytic surface, $-\Delta H^0_{ads}$ is highly negative and surface motion becomes restricted, indicating a high negative loss of entropy. Violation of either physical criteria indicated that the derived value for the adsorption parameter was meaningless in terms of physical perspective, thereby suggesting that an improper kinetic model was selected.

3. Results and discussion

3.1. Surface structure of the MnO_2/graphene sample

XPS was used to obtain the surface structure information of the MnO_2/graphene composite. The O1s spectrum was deconvoluted into four distinct curves, as shown in Fig. 1. These curves include the peaks of anhydrous compounds (Mn-O) at 529.31 eV and water molecule (H-O-H) peak at 532.40 eV. These findings agree with the literature values of 529.3–530.3 eV for MnO_2 and 531.8–532.8 eV for water [47]. The intensity of the 530.40 eV peak can be attributed to the presence of C-O [48]. The fourth peak exhibited a binding energy of 529.46 eV. Meng et al. [49] assigned a new binding energy peak to Mn-O-Si which was found on manganese containing zeolite synthesized using the hydrothermal method. Considering the similar synthesis method used in the present study, the new 529.46 eV peak can be reasonably ascribed to Mn-O-C. The presence of the Mn-O-C bond was also proven by

the FTIR results in our previous work [26]. The presence of Mn-O-C confirms that the active sites of graphene and the dispersed MnO_2 are strongly connected on the surface, thereby confirming the dual-site mechanism. In this mechanism, the two sites must be located sufficiently close to the surface to allow their adsorbed species to easily react with one other [50-52].

3.2. Steady-state kinetic study

High-temperature reactions would achieve high conversion for catalytic ozonation of toluene over the MnO_2/graphene composite [53]. Therefore, relatively low temperatures (295, 313, and 333 K) and high gas flow rate were selected for the reaction tests. All conversions of the toluene data were less than 15%, whereas those of ozone were typically more than 30% under the tested reaction condition. For reliability, the resulting kinetic data were only used to determine the kinetic parameters for toluene. Three kinetic models were developed based on the power law, L-H_s mechanism, and L-H_d mechanism.

3.2.1. Power law model

The power law model contained three unknown parameters (k, α, and β), as shown in Eq. (8) [54, 55].

$r_{tol} = kC_{tol}^{\alpha} C_{O_3}^{\beta}$	(8)

where r_{tol} is the steady-state reaction rate of toluene. C_{tol} and C_{O_3} are the steady-state concentrations of toluene and ozone, respectively. α and β are the orders with respect to toluene and ozone concentrations, respectively. Reaction data at each temperature point in Table 1 were fit to an expression as shown in Eq. (8) by using nonlinear least squares

regression analysis explained in Section *2.2 Data analysis* to determine the rate expression. The results of the fitting are shown in Table 2. The fitting analysis obtained an adjusted R^2 degree of fit values of 0.9, 0.96, and 0.96 for the three selected temperature points (295, 313 and 333 K). These results indicated that the power law model was well fitted. Both α and β values for different temperatures slightly differed, which could be due to experimental and statistical errors. The similar results were also found in the study on steady-state kinetic analysis of catalytic ozonation of acetone [10]. The apparent activation energy (E_a) of the reaction was determined to be 29.3±2.5 kJ mol^{-1} based on the derived reaction rate constant of each temperature point with Eq. (3) through linear regression (Fig. S1 for details). This value is close to the value (31 kJ mol^{-1}) obtained by Rezaei and Soltan [24] for catalytic ozonation of toluene over alumina-supported manganese oxide catalysts. The determined activation energy of 29.3±2.5 kJ mol^{-1} in the present study was lower than that for the homogeneous reaction (55.6 kJ mol^{-1}) between toluene and ozone, as reported by Toby et al. [56]; thus, under the current reaction condition, the catalytic ozonation of toluene over MnO_2/graphene was considered a heterogeneous reaction that occurred on the catalyst surface. Therefore, the Langmuir-Hinshelwood mechanism could be utilized to explain experimental observations [57-59].

3.2.2. L-H kinetic model development

In our previous work [26], we found that pristine graphene showed some activity for ozone decomposition while MnO_2 exhibited much higher decomposition rate than that on graphene (around 10 times), which was attributed to its superior ability to adsorb ozone [27]. Based on this, we concluded that MnO_2 would be much more active for ozone adsorption than graphene and serve as the active site for ozone adsorption when MnO_2/graphene composite

was used for catalytic ozonation. Therefore, in the present work, we proposed that MnO_2 (instead of graphene) was the active site for ozone adsorption during the kinetic modelling. Two kinetic models were developed based on L-H_s and L-H_d mechanisms. The elementary steps involved for both mechanisms are presented in Table 3. For the L-H_s mechanism, the proposed steps by Oyama et al. [10] as well as Rezaei and Soltan [24] were fully adopted and listed in the left of Table 3. Briefly, the L-H_s mechanism consists of two cycles: ozone decomposition, as shown in steps (1) to (3), and toluene equilibrated adsorption [step (4)], migration [step (5)], and activation [step (6)], which are involved in one another. Further steps after step (6) were assumed to be not significant from the kinetic point of view [10]. Given the presence of the migration step, active site balance only occurred on one type of active site (s1 ; i.e., MnO_2), whereas the other site (s2 ; i.e., graphene) was dismissed for kinetic expression development. Thus, the developed equation [Eq. (9)] [10, 24] could be considered as actual L-H_s mechanism-based kinetic expression.

$r_{tol} = K_{tol} \frac{k_1'[C_7H_8][O_3]^2}{(1+k_2'[O_3]+K_{tol}[C_7H_8])^3}$	(9)

where r_{tol} is the toluene reaction rate, K_{tol} is the product of two equilibrium adsorption constants in steps (4) and (5) [10]. k_2' is set as $\frac{k_1}{k_3}$, which is the reaction rate constant in step (1) divided by that of step (3). k_1' is defined as $k_5 k_2'$ which is the reaction rate constant in step (5) multiplied by k_2'.

We propose a novel kinetic model based on L-H_d mechanism, other than the L-H_s mechanism. The elementary steps involved in the former mechanism are shown in the right column of Table 3. The L-H_d model also consists of two cycles, which follow the conclusion

from the systematic study by Oyama et al. [10, 28], particularly with regard to the results of in situ Raman spectroscopy. The ozone decomposition cycle in the present study [i.e., steps (1)–(3)] is similar to a previously reported cycle [27, 28], and the difference originates from toluene. In the present study, the s2 (graphene) site can be used for toluene adsorption because two active sites exist [step (4)]. The adsorbed toluene molecule on the s2 (graphene) site can react with the adjacent atomic oxygen species [step (5)] formed by ozone decomposition; this process occurred in the first ozone cycle on the s1 (MnO_2) site, and step (5) in L-H_s was skipped in the proposed L-H_d mechanism. The well-designed catalyst renders the L-H_d mechanism as reasonable because of two advantages. First, the inherent π orbitals in graphene allow the toluene molecule to be adsorbed easily on the graphene surface by π-electron coupling between graphene and toluene. Lazar et al. [60] reported similar results, that is, toluene exhibits the highest affinity to graphene through combined experimental and computational (DFT) studies of seven organic molecules on graphene. These studies aimed to identify the magnitude and nature of the interaction.

Second, adsorbed toluene molecule can be activated by neighboring atomic oxygen species because of the strong connection between graphene and MnO_2. The presence of this connection was confirmed by the XPS results. With this strong connection and following the adjacent attack, the migration step shown in the L-H_s mechanism [step (5)] could be dismissed. As a result, the dual-site mechanism should be utilized to explain the surface reaction. On the basis of this L-H_d mechanism, both s1 and s2 active sites should be considered for the kinetic model development. The detailed derivation procedure is shown in later section. However, before the derivation, three assumptions were made and clarified.

First, the last step in the L-H_d mechanism can be considered a slow step for catalytic ozonation of toluene, and the following steps were kinetically meaningless [10, 24]. Therefore,

Eq. (10) was used to develop the rate of toluene removal, which includes both $s1$ (MnO_2) and $s2$ (graphene) sites. The concentration of both intermediates, $[C_7H_8 * s2]$ and $[O * s1]$, in the reaction rate expression could not be measured. These two variables need to be replaced by known or determinable ones.

$r_{tol} = r_5 = k_5[C_7H_8 * s2][O * s1]$	(10)

Second, step (4) is under the equilibrium adsorption state, which indicates that the forward reaction proceeds at the same rate as the reverse reaction [Eq. (11)].

$k_4[C_7H_8][s2] = k_{-4}[C_7H_8 * s2]$	(11)

where k_4 and k_{-4} represent the forward and reverse reaction constants in step (4), respectively. $[s2]$ is the concentration of vacant sites of $s2$ (graphene). $[C_7H_8]$ and $[C_7H_8 * s2]$ are the concentrations of toluene in the gas phase and adsorbed toluene on the active site $s2$ (graphene).

Third, the pseudo-steady-state hypothesis (PSSH) [61, 62] can be used to derive rate law, given that all data were collected under the steady-state conditions in the present study. Each species adsorbed on the surface is assumed to be a reactive intermediate. Consequently, the net rate of formation of species adsorbed on the surface is zero, as shown in Eqs. (12) and (13).

$\frac{d[O * s1]}{dt} = r_1 - r_2 - r_5 = 0$	(12)
$\frac{d[O_2 * s1]}{dt} = r_2 - r_3 = 0$	(13)

where $[O * s1]$ is the concentration of the atomic oxygen species intermediate adsorbed on

$s1$ (MnO_2) active sites. $[O_2 * s1]$ is the concentration of peroxide species adsorbed on s1 (MnO_2) active sites. r_i is the reaction rate corresponding to step (i) reaction listed in the right part of Table 3.

Two unknown variables, namely, $[C_7H_8 * s2]$ and $[O * s1]$, need to be replaced by other measurable factors to achieve the reaction rate expression for toluene removal. After starting with Eqn. (11), $[C_7H_8 * s2]$ can then be expressed as Eq. (14).

$[C_7H_8 * s2] = K_{tol}[C_7H_8][s2]$	(14)

where $K_{tol} = \frac{k_4}{k_{-4}}$ is the equilibrium adsorption constant of toluene on active site $s2$. The site balance on $s2$ was performed with $[s2]$ and $[C_7H_8 * s_2]$, that is $[s2] + [C_7H_8 * s_2] = 1$.

Substituting Eq. (14) to the $s2$ site balance equation, the concentration of vacant $s2$ site can be determined to be:

$[s2] = \frac{1}{1 + K_{tol}[C_7H_8]}$	(15)

By combining Eqs. (14) and (15), we can determine $[C_7H_8 * s2]$, the concentration of adsorbed toluene species on the $s2$ site (graphene), with measurable factor, concentration of toluene in the gas phase.

$[C_7H_8 * s2] = \frac{K_{tol}[C_7H_8]}{1 + K_{tol}[C_7H_8]}$	(16)

In the next step, we go back to Eq. (12) to replace $[O * s1]$. The concentration of the adsorbed atomic oxygen species can be expressed using two measurable factors ($[O_3]$ and

$[C_7H_8]$) and one undeterminable variable $[s1]$.

$$[O*s1]=\frac{k_1[O_3]}{k_2[O_3]+\frac{K_{tol}k_5[C_7H_8]}{1+K_{tol}[C_7H_8]}}[s1] \quad (17)$$

Similarly, the concentration of adsorbed peroxide intermediates can be expressed using two measurable factors ($[O_3]$ and $[C_7H_8]$) and one undeterminable variable $[s1]$, as shown in Eq. (18) by combining Eqs. (13) and (17),

$$[O_2*s1]=\frac{k_1k_2[O_3]^2}{k_2k_3[O_3]+\frac{k_3K_{tol}k_5[C_7H_8]}{1+K_{tol}[C_7H_8]}}[s1] \quad (18)$$

The concentration of vacant sites $[s1]$ can be eliminated by performing a total site balance on $s1$ with $[s1]$, $[O*s1]$, and $[O_2*s1]$, that is, $[s1]+[O*s1]+[O_2*s1]=1$.

Substituting Eqs. (17) and (18) to the site balance equation, we have

$$[s1]=\frac{1}{1+\frac{k_1[O_3]}{k_2[O_3]+\frac{K_{tol}k_5[C_7H_8]}{1+K_{tol}[C_7H_8]}}+\frac{k_1k_2[O_3]^2}{k_2k_3[O_3]+\frac{k_3K_{tol}k_5[C_7H_8]}{1+K_{tol}[C_7H_8]}}} \quad (19)$$

By combining Eqs. (17) and (19), we can derive one expression for the concentration of atomic oxygen species intermediate with measurable factors, as shown in Eq. (20).

$$[O*s1]=\frac{k_1[O_3]}{k_2[O_3]+\frac{K_{tol}k_5[C_7H_8]}{1+K_{tol}[C_7H_8]}+k_1[O_3]+\frac{k_1k_2[O_3]^2}{k_3}} \quad (20)$$

Substituting Eqs. (16) and (20) to Eq. (10), the reaction rate expression for toluene

removal under steady-state conditions can be expressed by the following equation:

$$r_{tol} = \frac{k_1 K_{tol} k_5 [C_7H_8][O_3]}{(1 + K_{tol}[C_7H_8])(k_2[O_3] + \frac{K_{tol} k_5 [C_7H_8]}{1 + K_{tol}[C_7H_8]} + k_1[O_3] + \frac{k_1 k_2 [O_3]^2}{k_3})} \quad (21)$$

3.2.3. Model discrimination and parameter estimation

The rate expressions derived from the L-H_s and L-H_d mechanisms, i.e., Eqs. (9) and (21), were fitted to kinetic data in Table 1 by using the method mentioned in *2.3. Data analysis*. The results are given in the parity plots, as shown in Fig. 2. The power law-based model results were also included in Fig. 2. Both the power law and the L-H_d model showed a reasonable agreement of the predicted reaction rate of toluene removal and the experimental reaction rate with a correlation coefficient near unity (r^2 = 0.8995 and 0.9165). This finding indicated that the proposed L-H_d mechanism with MnO_2 for ozone adsorption and toluene adsorption on graphene were consistent with kinetic measurements and may be used to represent the pattern of the experimental observations. The residual plot for the L-H_d model is presented in Fig. 3 to discriminate the selected mechanism and the derived model expression. The error was found to be randomly distributed, indicating that the correct rate expression should be chosen [57]. By contrast, the expression based on the L-H_s mechanism did not fit the experimental data, indicating that the catalytic ozonation of toluene over the MnO_2/graphene catalyst is non-single-site-governed.

Thus far, the L-H_d kinetic expression satisfied the mathematical criteria mentioned in Section *2.3. Data analysis*. The next criterion was evaluated from the physical point of view, which would be assessed based on the entropy and enthalpy of toluene adsorption. The estimated kinetic parameters for the L-H_d model are listed in Table 4. The reaction rate and equilibrium constants are listed in the left part by fitting Eq. (21) to the experimental results in

Table 1. Pre-exponential factors, activation energy, and entropy and enthalpy of toluene adsorption are shown in the right part, and these factors were determined by linear regression with the Arrhenius or Van't Hoff equation and the details of the derivation shown in Figs. S2–S6. As shown in Table 4, the pre-exponential factor for step (1) held a very large number, $1.50\times10^{19}\pm1.2\times10^{5}$, whereas the values for the following two steps involved in the ozone decomposition are low, namely, 4.4±2.1 and 26.0±18.8, indicating that the first step was much faster than the subsequent two steps. These results are consistent with the conclusion by Oyama et al. [27, 28] that step (1) by itself is faster than steps (2) and (3). Step (6) (the reaction between adsorbed intermediates) was considered a slow step for the catalytic ozonation of acetone [10]. In the present study, the same assumption was proposed. The activation energy for step (5), attack by intermediates on adjacent foreign sites, was found to be 43.9±14.3 kJ mol^{-1}, which is close to the value (48 kJ mol^{-1}) determined by Rezaei and Soltan for step (6), activation with intermediates on adjacent native sites (left part of Table 3) with the L-H_s mechanism [24]. This result suggested that the activation of adsorbed toluene on graphene by neighboring atomic oxygen species on MnO_2 was true in MnO_2-graphene dual-site catalyst. The pre-exponential factor for step (5) was relatively high ($5.77\pm0.04\times10^{3}$ mol $kg^{-1}s^{-1}$), leading to a relatively high reaction rate. However, the high activation energy (43.9±14.3 kJ mol^{-1}) for this step may partially cancel the accelerating influence from the pre-exponential factor on the reaction rate. In Table 4, the rate constants for step (5) were very low at all three measured temperature points ($(9.79\pm0.13)\times10^{-5}$, $(2.34\pm0.08)\times10^{-4}$, and $(1.05\pm0.06)\times10^{-3}$ mol kg^{-1} s^{-1}, respectively); hence, this step was the rate-determining step for the proposed L-H_d mechanism and confirmed the aforementioned assumption that step (5) could be considered a slow step for the catalytic ozonation of toluene. The activation energy of ozone adsorption in step (1) is higher than that of the surface reaction between the ozone

and adsorbed atomic oxygen species in step (2) or that of desorption of oxygen molecule in step (3). These findings may be attributed to the high activity of atomic oxygen species intermediates [63, 64]. The entropy and enthalpy of toluene adsorption were negative, which are common in adsorption. The estimated value for the entropy of toluene adsorption was -158.5±2.2 J mol^{-1} K^{-1}, which satisfied Eq. (6). The calculated value for the enthalpy of toluene adsorption was -57.5±1.3 kJ mol^{-1}, which is consistent with the reported value (−13.5 kcal mol^{-1}) of the adsorption enthalpy of toluene to graphene flakes by inverse gas chromatography measurement and further DFT calculation [60]. This finding confirmed our hypothesis that toluene is adsorbed on the graphene site in the MnO_2/graphene catalyst. Furthermore, the derived enthalpy satisfied the requirements of Eq. (7). Both physical constraints were met, indicating that the proposed model was physically meaningful. Therefore, the proposed L-H_d mechanism could be used to explain the catalytic ozonation of toluene over the MnO_2/graphene catalyst, that is, the entire reaction consists of two cycles: ozone decomposition over MnO_2 sites, which was the same as the classical explanation proposed by Oyama et al. [27, 28]; and toluene adsorption, which occurred on graphene sites. The two cycles were coupled by adjacent attack between adsorbed atomic oxygen species formed on the MnO_2 site in the first cycle and adsorbed toluene molecule on the graphene site in the second cycle. The strong connection between MnO_2 and graphene facilitated the occurrence of surface reaction between neighboring sites.

4. Conclusion

In this work, other than the classic Langmuir-Hinshelwood single-site-based model, a novel Langmuir-Hinshelwood dual-site-based mechanism was proposed to explain the experimental observation in the catalytic ozonation of toluene over the MnO_2/graphene

catalyst. Steady-state kinetic study was conducted to validate the hypothesis. The strong connection between MnO_2 and graphene sites on the surface facilitated adjacent attack and enabled the dual-site mechanism. Low apparent activation energy was determined by the empirical power law model, indicating that the catalytic ozoation reaction was heterogeneous and could be explained by the Langmuir-Hinshelwood mechanism. The L-H_s mechanism did not fit the experimental data, indicating that the reaction was non-single-site-governed. With the proposed L-H_d mechanism, the mathematical and physical criteria can be met, suggesting that the reaction can be well described by the L-H_d mechanism. This mechanism consisted of two cycle–ozone decomposition over MnO_2 sites and toluene adsorption on graphene sites. The two cycles were coupled by adjacent attack between adsorbed atomic oxygen formed in the first cycle and adsorbed toluene molecule from the second cycle. This study provides new insights into catalytic ozonation of toluene over the MnO_2/graphene catalyst in a closely mechanistic view.

Acknowledgements

This work was supported by the Science and Technology Development Fund from Macau SAR (FDCT-098/2015/A3), and the Start-up Research Grant (SRG2015-00057-FST) from Research & Development Office at University of Macau.

References

[1] M. Tokumura, M. Shibusawa, Y. Kawase, Dynamic simulation of degradation of toluene in waste gas by the photo-Fenton reaction in a bubble column[J]. Chem. Eng. Sci., 2013, 100 212-224.
[2] H. Huang, W. Li, Destruction of toluene by ozone-enhanced photocatalysis: Performance and mechanism[J]. Appl. Catal., B, 2011, 102 (3-4): 449-453.
[3] J. Kim, P. Zhang, J. Li, J. Wang, P. Fu, Photocatalytic degradation of gaseous toluene and ozone under UV254+185 nm irradiation using a Pd-deposited TiO2 film[J]. Chem. Eng. J., 2014, 252 337-345.
[4] C. Subrahmanyam, A. Renken, L. Kiwi-Minsker, Catalytic non-thermal plasma reactor for abatement of toluene[J]. Chem. Eng. J., 2010, 160 (2): 677-682.
[5] E. Rezaei, J. Soltan, N. Chen, Catalytic oxidation of toluene by ozone over alumina supported manganese oxides: Effect of catalyst loading[J]. Appl. Catal., B, 2013, 136-137 239-247.
[6] H. Einaga, Y. Teraoka, A. Ogata, Catalytic oxidation of benzene by ozone over manganese oxides supported on USY zeolite[J]. J. Catal., 2013, 305 227-237.
[7] M. Stoyanova, P. Konova, P. Nikolov, A. Naydenov, S. Christoskova, D. Mehandjiev, Alumina-supported nickel oxide for ozone decomposition and catalytic ozonation of CO and VOCs[J]. Chem. Eng. J., 2006, 122 (1–2): 41-46.
[8] A. Changsuphan, M.I.B.A. Wahab, N.T. Kim Oanh, Removal of benzene by ZnO nanoparticles coated on porous adsorbents in presence of ozone and UV[J]. Chem. Eng. J., 2012, 181-182 215-221.
[9] H. Huang, X. Ye, W. Huang, J. Chen, Y. Xu, M. Wu, Q. Shao, Z. Peng, G. Ou, J. Shi, X. Feng, Q. Feng, H. Huang, P. Hu, D.Y.C. Leung, Ozone-catalytic oxidation of gaseous benzene over MnO2/ZSM-5 at ambient temperature: Catalytic deactivation and its suppression[J]. Chem. Eng. J., 2015, 264 24-31.
[10] C. Reed, Y. Xi, S.T. Oyama, Distinguishing between reaction intermediates and spectators: A kinetic study of acetone oxidation using ozone on a silica-supported manganese oxide catalyst[J]. J. Catal., 2005, 235 (2): 378-392.
[11] C.W. Kwong, C.Y.H. Chao, K.S. Hui, M.P. Wan, Removal of VOCs from indoor environment by ozonation over different porous materials[J]. Atmos. Environ., 2008, 42 (10): 2300-2311.
[12] C.W. Kwong, C.Y.H. Chao, Fly-ash products from biomass co-combustion for VOC control[J]. Bioresour. Technol., 2010, 101 (3): 1075-1081.
[13] C.H. Perng, I.L. Cheng, I.C. Wang, M.S. Chou, Ozonation of odorous compounds in gases emitted from rubber processing industries[J]. Aerosol Air Qual. Res., 2011, 11 (1): 51-58.
[14] H. Einaga, S. Yamamoto, N. Maeda, Y. Teraoka, Structural analysis of manganese oxides supported on SiO2 for benzene oxidation with ozone[J]. Catal. Today, 2015, 242 (PB): 287-293.
[15] H. Einaga, S. Futamura, Oxidation behavior of cyclohexane on alumina-supported manganese oxides with ozone[J]. Appl. Catal., B, 2005, 60 (1-2): 49-55.
[16] K.S. Hui, C.W. Kwong, C.Y.H. Chao, Methane emission abatement by Pd-ion-exchanged zeolite 13X with ozone[J]. Energy Environ. Sci., 2010, 3 (8): 1092-1098.
[17] E. Rezaei, J. Soltan, Low temperature oxidation of toluene by ozone over MnOx/γ-alumina and MnOx/MCM-41 catalysts[J]. Chem. Eng. J., 2012, 198–199 482-490.
[18] E. Sahle-Demessie, V.G. Devulapelli, Vapor phase oxidation of dimethyl sulfide with ozone over V2O5/TiO2 catalyst[J]. Appl. Catal., B, 2008, 84 (3–4): 408-419.
[19] Q. Sun, L. Li, H. Yan, X. Hong, K.S. Hui, Z. Pan, Influence of the surface hydroxyl groups of MnOx/SBA-15 on heterogeneous catalytic ozonation of oxalic acid[J]. Chem. Eng. J., 2014, 242 348-356.
[20] C. Reed, Y.K. Lee, S. Ted Oyama, Structure and oxidation state of silica-supported manganese oxide catalysts and reactivity for acetone oxidation with ozone[J]. J. Phys. Chem. B, 2006, 110 (9): 4207-4216.
[21] Y. Xi, C. Reed, Y.K. Lee, S.T. Oyama, Acetone oxidation using ozone on manganese oxide catalysts[J]. J. Phys. Chem. B, 2005, 109 (37): 17587-17596.
[22] H. Einaga, A. Ogata, Catalytic oxidation of benzene in the gas phase over alumina-supported silver catalysts[J]. Environ. Sci. Technol., 2010, 44 (7): 2612-2617.
[23] H. Einaga, N. Maeda, Y. Nagai, Comparison of catalytic properties of supported metal oxides

for benzene oxidation using ozone[J]. Catal. Sci. Technol., 2015, 5 (6): 3147-3158.
[24] E. Rezaei, J. Soltan, EXAFS and kinetic study of MnOx/γ-alumina in gas phase catalytic oxidation of toluene by ozone[J]. Appl. Catal., B, 2014, 148–149 70-79.
[25] Y.T. Lai, T.C. Chen, Y.K. Lan, B.S. Chen, J.H. You, C.M. Yang, N.C. Lai, J.H. Wu, C.S. Chen, Pt/SBA-15 as a Highly Efficient Catalyst for Catalytic Toluene Oxidation[J]. ACS Catal. , 2014, 4 (11): 3824-3836.
[26] M. Hu, K.S. Hui, K.N. Hui, Role of graphene in MnO2/graphene composite for catalytic ozonation of gaseous toluene[J]. Chem. Eng. J., 2014, 254 237-244.
[27] W. Li, S.T. Oyama, Mechanism of ozone decomposition on a manganese oxide catalyst 2. Steady-state and transient kinetic studies[J]. J. Am. Chem. Soc., 1998, 120 (35): 9047-9052.
[28] W. Li, G.V. Gibbs, S.T. Oyama, Mechanism of ozone decomposition on a manganese oxide catalyst. 1. In situ Raman spectroscopy and Ab initio molecular orbital calculations[J]. J. Am. Chem. Soc., 1998, 120 (35): 9041-9046.
[29] D. Pakhare, V. Schwartz, V. Abdelsayed, D. Haynes, D. Shekhawat, J. Poston, J. Spivey, Kinetic and mechanistic study of dry (CO2) reforming of methane over Rh-substituted La2Zr2O7 pyrochlores[J]. J. Catal., 2014, 316 78-92.
[30] T.Y. Ma, S.Z. Qiao, Acid-base bifunctional periodic mesoporous metal phosphonates for synergistically and heterogeneously catalyzing CO2 conversion[J]. ACS Catal. , 2014, 4 (11): 3847-3855.
[31] D. Shi, J. Faria, T.N. Pham, D.E. Resasco, Enhanced activity and selectivity of Fischer-Tropsch synthesis catalysts in water/oil emulsions[J]. ACS Catal. , 2014, 4 (6): 1944-1952.
[32] A.A. Hakeem, M. Li, R.J. Berger, F. Kapteijn, M. Makkee, Kinetics of the high temperature water–gas shift over Fe2O3/ZrO2, Rh/ZrO2 and Rh/Fe2O3/ZrO2[J]. Chem. Eng. J., 2015, 263 427-434.
[33] K.S. Hui, K.N. Hui, D.A. Dinh, C.H. Tsang, Y.R. Cho, W. Zhou, X. Hong, H.-H. Chun, Green synthesis of dimension-controlled silver nanoparticle–graphene oxide with in situ ultrasonication[J]. Acta Mater., 2014, 64 326-332.
[34] M. Li, K.N. Hui, K.S. Hui, S.K. Lee, Y.R. Cho, H. Lee, W. Zhou, S. Cho, C.Y.H. Chao, Y. Li, Influence of modification method and transition metal type on the physicochemical properties of MCM-41 catalysts and their performances in the catalytic ozonation of toluene[J]. Appl. Catal., B, 2011, 107 (3–4): 245-252.
[35] M.P. Wan, K.S. Hui, C.Y.H. Chao, C.W. Kwong, Catalytic combustion of methane with ozone using Pd-exchanged zeolite X: Experimental investigation and kinetics model[J]. Combust. Sci. Technol., 2010, 182 (10): 1429-1445.
[36] U. Oemar, A. Ming Li, K. Hidajat, S. Kawi, Mechanism and kinetic modeling for steam reforming of toluene on La0.8Sr0.2Ni0.8Fe0.2O3 catalyst[J]. AIChE J., 2014, 60 (12): 4190-4198.
[37] M.M. Fathi, P. Pereira-Almao, Kinetic modeling of arab light vacuum residue upgrading by aquaprocessing at high space velocities[J]. Ind. Eng. Chem. Res., 2013, 52 (2): 612-623.
[38] R.M.F. Bezerra, I. Fraga, A.A. Dias, Utilization of integrated Michaelis-Menten equations for enzyme inhibition diagnosis and determination of kinetic constants using Solver supplement of Microsoft Office Excel[J]. Comput. Methods. Programs. Biomed., 2013, 109 (1): 26-31.
[39] M.J. Ferner, G. Müller, C. Schumann, P. Kampeis, R. Ulber, H. Raddatz, Immobilisation of glycosidases from commercial preparation on magnetic beads. Part 1. Characterisation of immobilised glycosidases with a particular emphasis on ß-glucosidase[J]. J. Mol. Catal. B: Enzym., 2016, 123 23-28.
[40] C. Huang, Y.Y. Li, L.P. Liu, H. Wu, M.H. Zong, W.Y. Lou, Kinetics and mechanism analysis on microbial oil production by Trichosporon fermentans in rice straw hydrolysate[J]. Ind. Eng. Chem. Res., 2014, 53 (49): 19034-19043.
[41] K. Baig, B. Kvamme, T. Kuznetsova, J. Bauman, Impact of water film thickness on kinetic rate of mixed hydrate formation during injection of CO2 into CH4 hydrate[J]. AIChE J., 2015, 61 (11): 3944-3957.
[42] G.F. Froment, Single event kinetic modeling of complex catalytic processes[J]. Cat. Rev. - Sci. Eng. , 2005, 47 (1): 83-124.
[43] G.F. Froment, On fundamental kinetic equations for chemical reactions and processes[J]. Curr. Opin. Chem. Eng., 2014, 5 1-6.

[44] S. Mukherjee, M.A. Vannice, Solvent effects in liquid-phase reactions II. Kinetic modeling for citral hydrogenation[J]. J. Catal., 2006, 243 (1): 131-148.
[45] M.P. Heynderickx, J.W. Thybaut, H. Poelman, D. Poelman, G.B. Marin, Kinetic modeling of the total oxidation of propane over CuO-CeO2/γ-Al2O3[J]. Appl. Catal., B, 2010, 95 (1–2): 26-38.
[46] J. Bedia, J.M. Rosas, J. Rodríguez-Mirasol, T. Cordero, Pd supported on mesoporous activated carbons with high oxidation resistance as catalysts for toluene oxidation[J]. Appl. Catal., B, 2010, 94 (1–2): 8-18.
[47] D. Yan, P. Yan, S. Cheng, J. Chen, R. Zhuo, J. Feng, G.a. Zhang, Fabrication, In-Depth Characterization, and Formation Mechanism of Crystalline Porous Birnessite MnO2 Film with Amorphous Bottom Layers by Hydrothermal Method[J]. Cryst. Growth Des., 2009, 9 (1): 218-222.
[48] O. García-Valdez, R. Ledezma-Rodríguez, E. Saldívar-Guerra, L. Yate, S. Moya, R.F. Ziolo, Graphene oxide modification with graft polymers via nitroxide mediated radical polymerization[J]. Polym., 2014, 55 (10): 2347-2355.
[49] Y. Meng, H.C. Genuino, C.-H. Kuo, H. Huang, S.-Y. Chen, L. Zhang, A. Rossi, S.L. Suib, One-Step Hydrothermal Synthesis of Manganese-Containing MFI-Type Zeolite, Mn–ZSM-5, Characterization, and Catalytic Oxidation of Hydrocarbons[J]. J. Am. Chem. Soc., 2013, 135 (23): 8594-8605.
[50] A. Siahvashi, A.A. Adesina, Kinetic Study of Propane CO2 Reforming over Bimetallic Mo–Ni/Al2O3 Catalyst[J]. Ind. Eng. Chem. Res., 2013, 52 (44): 15377-15386.
[51] R.A. van Santen, M.M. Ghouri, S. Shetty, E.M.H. Hensen, Structure sensitivity of the Fischer-Tropsch reaction; molecular kinetics simulations[J]. Catal. Sci. Technol., 2011, 1 (6): 891-911.
[52] B. Qiao, J. Liu, Y.G. Wang, Q. Lin, X. Liu, A. Wang, J. Li, T. Zhang, J. Liu, Highly Efficient Catalysis of Preferential Oxidation of CO in H2-Rich Stream by Gold Single-Atom Catalysts[J]. ACS Catal. , 2015, 5 (11): 6249-6254.
[53] J. Li, H. Na, X. Zeng, T. Zhu, Z. Liu, In situ DRIFTS investigation for the oxidation of toluene by ozone over Mn/HZSM-5, Ag/HZSM-5 and Mn–Ag/HZSM-5 catalysts[J]. Appl. Surf. Sci., 2014, 311 690-696.
[54] Y. Khan, M. Marin, R. Karinen, J. Lehtonen, J. Kanervo, 1-Butanol dehydration in microchannel reactor: Kinetics and reactor modeling[J]. Chem. Eng. Sci., 2015, 137 740-751.
[55] C. Ledesma, J. Yang, D. Chen, A. Holmen, Recent approaches in mechanistic and kinetic studies of catalytic reactions using SSITKA technique[J]. ACS Catal. , 2014, 4 (12): 4527-4547.
[56] S. Toby, L.J. Van de Burgt, F.S. Toby, Kinetics and chemiluminescence of ozone-aromatic reactions in the gas phase[J]. J. Phys. Chem., 1985, 89 (10): 1982-1986.
[57] H.S. Fogler, Elements of Chemical Reaction Engineering, 4th ed., Prentice Hall, Upper Saddle River, NJ, USA., 2006.
[58] S.M. Lang, I. Fleischer, T.M. Bernhardt, R.N. Barnett, U. Landman, Low-Temperature CO Oxidation Catalyzed by Free Palladium Clusters: Similarities and Differences to Pd Surfaces and Supported Particles[J]. ACS Catal. , 2015, 5 (4): 2275-2289.
[59] D. Meng, W. Zhan, Y. Guo, Y. Guo, L. Wang, G. Lu, A Highly Effective Catalyst of Sm-MnOx for the NH3-SCR of NOx at Low Temperature: Promotional Role of Sm and Its Catalytic Performance[J]. ACS Catal. , 2015, 5 (10): 5973-5983.
[60] P. Lazar, F. Karlický, P. Jurečka, M. Kocman, E. Otyepková, K. Šafářová, M. Otyepka, Adsorption of Small Organic Molecules on Graphene[J]. J. Am. Chem. Soc., 2013, 135 (16): 6372-6377.
[61] B.L. Liu, M.L. Wang, Kinetic study of S-alkylation of 2-mercaptobenzimidazole with allyl bromide in a two-phase medium[J]. Ind. Eng. Chem. Res., 2008, 47 (6): 1784-1792.
[62] R. De Bruycker, S.P. Pyl, M.F. Reyniers, K.M. Van Geem, G.B. Marin, Microkinetic model for the pyrolysis of methyl esters: From model compound to industrial biodiesel[J]. AIChE J., 2015, 61 (12): 4309-4322.
[63] L. Shi, X.Q. Zhu, Y. Su, W.Z. Weng, H. Feng, X.D. Yi, Z.X. Liu, H.L. Wan, Synergetic effect of VOx and TeOx species in mesoporous SiO2 on selective oxidation of propane to acrolein[J]. J. Catal., 2013, 307 316-326.
[64] C. Fan, Y.A. Zhu, M.L. Yang, Z.J. Sui, X.G. Zhou, D. Chen, Density Functional Theory-Assisted Microkinetic Analysis of Methane Dry Reforming on Ni Catalyst[J]. Ind. Eng.

Chem. Res., 2015, 54 (22): 5901-5913.

Table captions

Table 1 Experimental conditions and results of the steady-state kinetic study.

Table 2 Results of nonlinear least squares regression based on power law expressions.

Table 3 Elementary steps in the catalytic ozonation of toluene over MnO_2/graphene catalyst based on the Langmuir-Hinshelwood single-site (L-H_s) and dual-site (L-H_d) mechanism. Estimated kinetic parameters with their 95% confidence intervals for the L-H_d model.

Figure captions

Fig. 1 XPS spectra at the binding energy range for O1s.

Fig. 2 Parity plot of the experimental and predicted reaction rates.

Fig. 3 Residual plot of the model based on the L-H_d mechanism.

Table 1

Experimental conditions and results of the steady-state kinetic study[a].

Temperature	$C_{i,0}$ (mol m^{-3})[b]		C_i (mol m^{-3})[c]		X_{tol}[d]	r_{tol}[e]
(K)	Toluene	O_3	Toluene	O_3	(%)	(mol $kg^{-1}s^{-1}$)
295	0.0124	0.0659	0.0112	0.0270	9.39	3.47×10^{-5}
295	0.0165	0.0659	0.0149	0.0379	9.49	4.67×10^{-5}
295	0.0206	0.0659	0.0188	0.0451	8.68	5.34×10^{-5}
295	0.0247	0.0659	0.0229	0.0477	7.32	5.41×10^{-5}
295	0.0288	0.0659	0.0270	0.0503	6.36	5.48×10^{-5}
295	0.0329	0.0659	0.0308	0.0512	6.45	6.35×10^{-5}
313	0.0124	0.0659	0.0108	0.0433	12.33	4.55×10^{-5}
313	0.0165	0.0659	0.0148	0.0461	10.07	4.96×10^{-5}
313	0.0206	0.0659	0.0185	0.0476	10.37	6.38×10^{-5}
313	0.0247	0.0659	0.0225	0.0491	9.10	6.72×10^{-5}
313	0.0288	0.0659	0.0261	0.0498	9.40	8.11×10^{-5}
313	0.0329	0.0659	0.0301	0.0517	8.63	8.50×10^{-5}
333	0.0124	0.0659	0.0109	0.0179	11.37	4.20×10^{-5}
333	0.0165	0.0659	0.0147	0.0176	10.78	5.31×10^{-5}
333	0.0206	0.0659	0.0176	0.0187	14.28	8.79×10^{-5}
333	0.0247	0.0659	0.0211	0.0232	14.50	1.07×10^{-4}
333	0.0288	0.0659	0.0247	0.0187	14.48	1.25×10^{-4}
333	0.0329	0.0659	0.0286	0.0231	13.21	1.30×10^{-4}

[a] The reaction test was conducted on 64.6 wt% MnO_2/graphene catalyst with a weight of 8.36×10^{-5} kg and total gas flow rate of 2.5×10^{-6} m^3 s^{-1}; The average value of three sets of independent experiments (deviations within ±5%) was reported using three different batches of the sample.

[b] Feed concentration of toluene and ozone, $C_{i,0}$, i is tol or O_3, which refers to toluene or ozone;

[c] Outlet concentration of toluene and ozone, C_i, i is tol or O_3 which refers to toluene or ozone;

[d] Toluene conversion, $X_{tol} = \frac{C_{tol,0} - C_{tol}}{C_{tol,0}} \times 100\%$ C_{tol} is toluene concentration in outlet.

[e] The toluene reaction rate under the steady- state conditions (mol kg^{-1} s^{-1}), $r_{tol} = \frac{C_{tol,0} v X_{tol}}{W}$,

$C_{tol,0}$: feed toluene concentration (mol m^{-3}); *v*: total gas flow rate (m^3 s^{-1}); X_{tol}: toluene conversion; and W: catalyst weight (kg);

Table 2

Results of nonlinear least squares regression based on power law expressions.

T (K)	k	α	β	Adj. R^2
Power law rate expression: $r_{tol} = kC_{tol}^{\alpha}C_{O_3}^{\beta}$				
295	$(3.25\pm0.71)\times10^{-3}$	0.6334±0.062	0.5509±0.061	0.9
313	$(6.18\pm1.03)\times10^{-3}$	0.6983±0.058	0.5980±0.047	0.96
333	$(1.27\pm0.25)\times10^{-2}$	0.6699±0.049	0.5839±0.039	0.96

Table 3

Elementary steps in the catalytic ozonation of toluene over the MnO_2/graphene catalyst, based on the Langmuir-Hinshelwood single-site (L-H_s) and dual-site (L-H_d) mechanisms[a].

Step no.	L-H_s mechanism elementary steps[b]	***Step no.***	L-H_d mechanism elementary steps
1	$O_3 + s1 \rightarrow O_2 + O*s1$	***1***	$O_3 + s1 \rightarrow O_2 + O*s1$
2	$O_3 + O*s1 \rightarrow O_2 + O_2*s1$	***2***	$O_3 + O*s1 \rightarrow O_2 + O_2*s1$
3	$O_2*s1 \rightarrow O_2 + s1$	***3***	$O_2*s1 \rightarrow O_2 + s1$
4	$C_7H_8 + s2 \Leftrightarrow C_7H_8*s2$	***4***	$C_7H_8 + s2 \Leftrightarrow C_7H_8*s2$
5	$C_7H_8*s2 + s1 \Leftrightarrow C_7H_8*s1 + s2$	***5***	$C_7H_8*s2 + O*s1 \rightarrow$ *products*
6	$C_7H_8*s1 + O*s1 \rightarrow$ *products*		

[a] $s1$ refers to MnO_2 sites, and $s2$ denotes graphene sites on the catalyst surface.

[b] L-H_s mechanism elementary steps were adopted from reference [10, 24].

Table 4

Estimated kinetic parameters with their 95% confidence intervals for the L-H_d model.[a]

Rate Constant	Temperature (K)			A_i[b]	E_a[c]	ΔH[d]	ΔS[e]
	295	313	333	(mol kg^{-1} s^{-1})	(kJ mol^{-1})	(kJ mol^{-1})	(J mol^{-1} K^{-1})
k_1 / 10^6	1.37±0.19	26.4±3.4	45.2±5.1	$1.50\times10^{19}\pm1.2\times10^{5}$	72.6±56.7	-	-
k_2	0.80±0.03	0.88±0.01	0.97±0.03	4.4±2.1	4.2±0.4	-	-
k_3	0.27±0.01	0.44±0.01	0.48±0.01	26.0±18.8	10.9±11.6	-	-
K_{tol}	80.4±5.2	21.6±2.7	5.5±0.47	-	-	-57.5±1.3	-158.5±2.2
k_5 / 10^{-5}	9.79±0.13	23.4±0.81	105±6.3	$5.77\pm0.04\times10^{3}$	43.9±14.3	-	-

[a] Rate constant attained by fitting Eq. (21) to reaction data in Table 1;

[b] Pre-exponential factor A_i, and [c] activation energy E_a were determined by Eq. (3) with linear regression;

[d] Enthalpy ΔH and [e] entropy ΔS of toluene adsorption on the MnO_2/graphene catalyst were determined by Eq. (4) with linear regression;

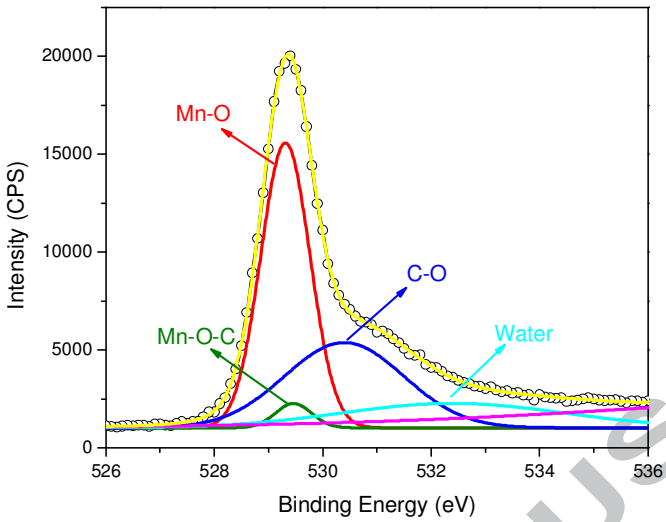

Fig. 1 XPS spectra at the binding energy range for O1s. Small, open circles in black are the measured experiment points. The solid line in yellow is the sum of all the peak fittings.

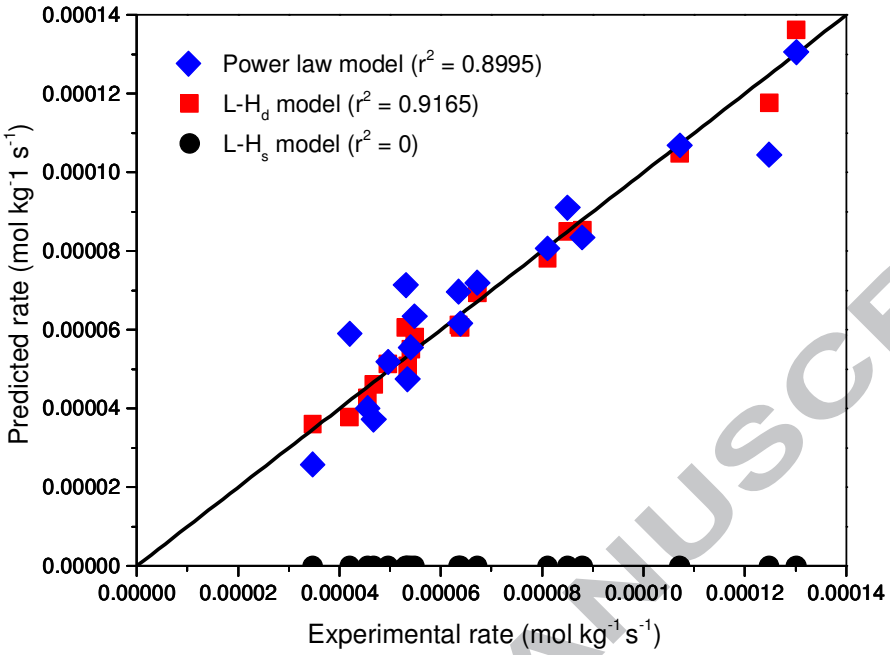

Fig. 2. Parity plot of the experimental and the predicted reaction rates. Experimental condition and the rates were given in Table 1. Predicted rates were obtained by fitting experimental data in Table 1 with Eqs. (8), (9) and (21) for power law, L-H_s and L-H_d model, respectively. The corresponding parameter estimates were given in Table 2 and 4.

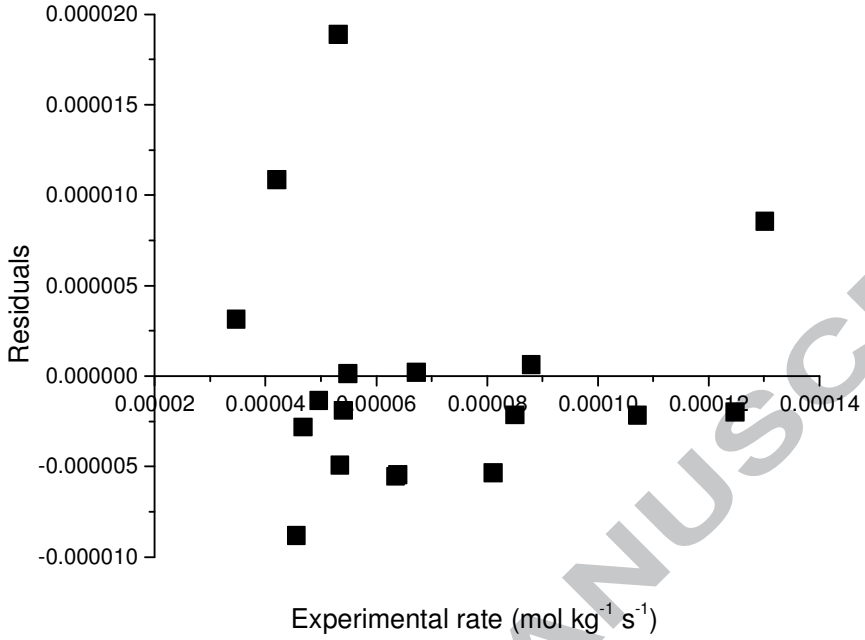

Fig. 3. Residual plot of the model based on the L-H_d mechanism.

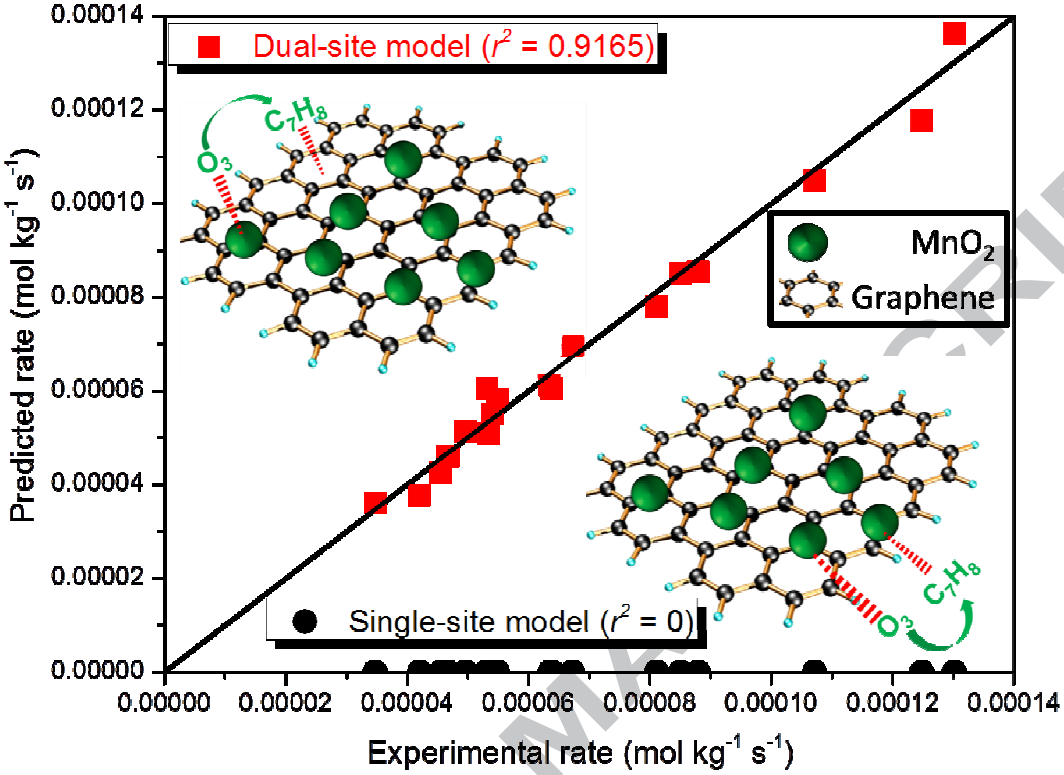

Graphical abstract

Highlights

- Novel dual-site modeling was performed for catalytic ozonation of toluene
- Strong connection confirmed by XPS made adjacent attack possible
- Model predictions were validated with experimental results and reported data
- Understanding the catalytic ozonation of toluene in a closely mechanistic view